Int J CARS (2013) 8:1063–1072
DOI 10.1007/s11548-013-0904-9

ORIGINAL ARTICLE

Improving N-wire phantom-based freehand ultrasound calibration

Guillermo Carbajal · Andras Lasso · Álvaro Gómez · Gabor Fichtinger

Received: 10 January 2013 / Accepted: 28 May 2013 / Published online: 28 July 2013
© CARS 2013

Abstract
Purpose Freehand tracked ultrasound imaging is an inexpensive non-invasive technique used in several guided interventions. This technique requires spatial calibration between the tracker and the ultrasound image plane. Several calibration devices (a.k.a. phantoms) use N-wires that are convenient for automatic procedures since the segmentation of fiducials in the images and the localization of the middle wires in space are straightforward and can be performed in real time. The procedures reported in literature consider only the spatial position of the middle wire. We investigate if better results can be achieved if the information of all the wires is equally taken into account. We also evaluated the precision and accuracy of the implemented methods to allow comparison with other methods.
Methods We consider a cost function based on the in-plane errors between the intersection of all the wires with the image plane and their respective segmented points in the image. This cost function is minimized iteratively starting from a seed computed with a closed-form solution based on the middle wires.
Results Mean calibration precision achieved with the N-wire phantom was about 0.5 mm using a shallow probe, and mean accuracy was around 1.4 mm with all implemented methods. Precision was about 2.0 mm using a deep probe.
Conclusions Precision and accuracy achieved with the N-wire phantom and a shallow probe are at least comparable to that obtained with other methods traditionally considered more precise. Calibration using N-wires can be done more consistently if the parameters are optimized with the proposed cost function.

Keywords Freehand ultrasound · Calibration · N-wire phantom · Accuracy

G. Carbajal · Á. Gómez
Facultad de Ingeniería, Universidad de la República, Montevideo, Uruguay
e-mail: carbajal@cs.queensu.ca

A. Lasso · G. Fichtinger (✉)
Laboratory for Percutaneous Surgery, School of Computing, Queen's University, Kingston, Canada
e-mail: gabor@cs.queensu.ca

Introduction

Freehand tracked ultrasound imaging is an inexpensive, safe, non-invasive technique for several guided interventions such as needle insertions, biopsies and ablations among others. Tracking allows registering ultrasound with other modalities for planning and navigation. It also enables to record, reconstruct and visualize large 3D volumes using conventional ultrasound probes.

To build a tracked ultrasound system, the most common method is to rigidly attach a position marker to a conventional ultrasound probe (Fig. 1). A tracking device (e.g., optical or electro-magnetic tracker) continuously monitors the marker and provides the position and orientation of the probe-marker in tracker coordinate system (*Tracker,* abbreviated as T) in real time. Spatial accuracy of the tracked US system mainly depends on how accurately the position and orientation of the ultrasound (US) scan plane (*US* coordinate system, abbreviated as U) with respect to the probe-marker's coordinate system (*Probe*, abbreviated as P) is determined. Probe calibration is the procedure used to get the ${}^{\mathbf{P}}_{\mathbf{U}}\mathbf{T}$ transformation that relates points in the *US* coordinate system with points in the *Probe* coordinate system.

Most calibration procedures require a calibration phantom designed to provide a set of fiducials that can be accurately

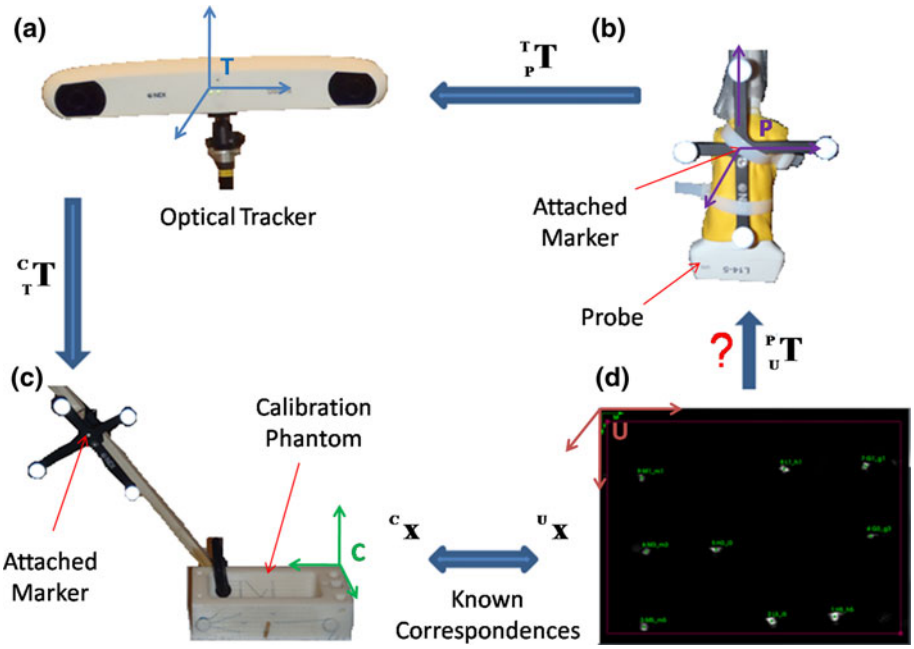

Fig. 1 Transformations involved in the image to probe calibration procedure: **a** sensor of the optical tracking device **b** probe with an attached marker **c** calibration phantom with an attached marker **d** N-wire intersection points visible in the ultrasound image

localized both in the ultrasound images and in the calibration phantom model. Calibration phantoms can range from single-bead and cross-wire phantoms [9], to multiple N-wire phantoms [1–4] and also more complex devices such as the Cambridge phantom [13]. Calibration without a phantom has also been investigated [11]. Detailed reviews on freehand ultrasound calibration are available in [6,10].

The N-wire geometry was originally used for image to patient registration with stereotactic frames and computed tomography (CT) [1] and was subsequently used in other domains (robotics, MRI, ultrasound calibration, etc.) to compute transformations. For devices that provide high-resolution, distortion-free images, the N-wire-based calibration operation is simple and high accuracy can be achieved.

However, due to the thickness of the US image slice, the localization accuracy in US imaging is usually highly anisotropic. In-plane localization, error can be as much as a magnitude smaller than out-of-plane error. Also, if the actual speed of sound is not the same as the speed of sound assumed by the US device, then the image may be distorted.

N-wire phantoms are still a compelling choice for US calibration due to the following reasons:

- Intersection between N-wires and the image plane appear as collinear bright spots in the US image, which can be segmented accurately, robustly and automatically in real time.
- It is possible to compute the intersection of the middles wires with the image plane in the calibration phantom coordinate system if the phantom geometry and the wire intersection positions in the US image plane are known. The intersection of the middle wire with the image plane in the calibration phantom coordinate system is computed using Eq. 1 [3]. Parameters of the equation are illustrated in Fig. 2.

$$ {}^{C}\mathbf{x}_2 = {}^{C}\mathbf{a} + \frac{\left\| {}^{U}\mathbf{x}_3 - {}^{U}\mathbf{x}_2 \right\|}{\left\| {}^{U}\mathbf{x}_3 - {}^{U}\mathbf{x}_1 \right\|} \left({}^{C}\mathbf{d} - {}^{C}\mathbf{a} \right) \quad (1) $$

This provides a simple and operator-independent mechanism to get correspondences between points in the *Calibration Phantom* coordinate system (abbreviated as *C*) and points in the *US* coordinate system that allows resolving the freehand ultrasound calibration problem.

Chen et al. [3] proposed a method to perform the calibration automatically through a closed-form solution. However, the method has several strong limitations:

1. The calibration transformation computed by the method described in [3] is not necessarily orthogonal. Most often we obtain skewed (non-orthogonal) calibration matrix as a result when the input images are very low quality and fiducial line detection is inaccurate. As the calibration result may be non-orthogonal, we have to apply an orthogonalization operation. This is necessary for two reasons:
   a. To have a calibration matrix in conformity with the model described in [6] and explained in "Calibration transformation modeling" of this document.
   b. From a practical point of view, most of the software that utilizes the calibration matrix can only work with orthogonal matrices (e.g., not prepared for rendering skewed images).

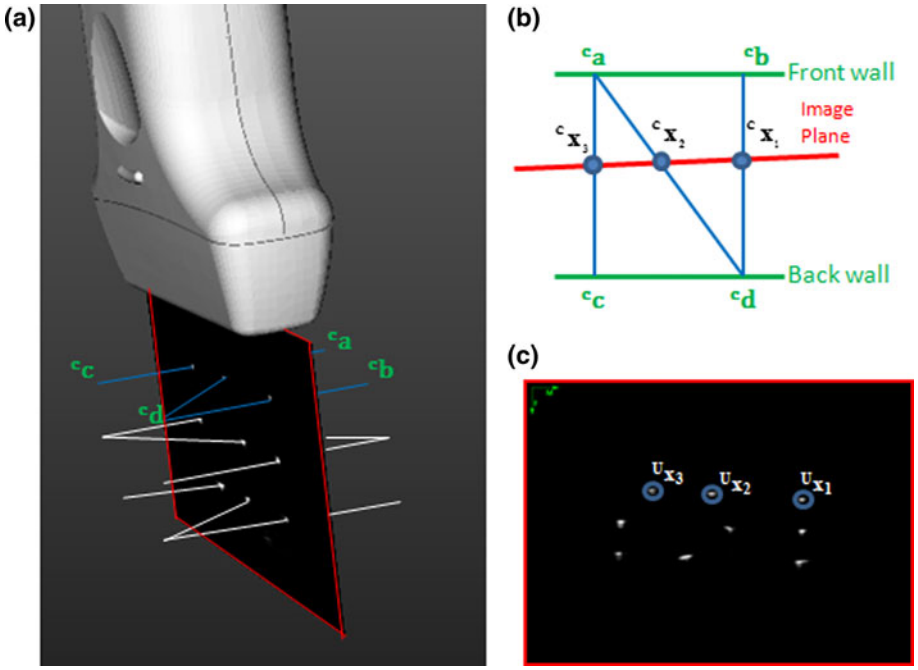

Fig. 2 **a** Outline of the three layers of N-wires used for the calibration. Image plane is shown in red. Image plane kept approximately orthogonal to the wires. **b** Sketch of the top N-wire in the calibration phantom. ${}^{C}\mathbf{x}_1, {}^{C}\mathbf{x}_2$ and ${}^{C}\mathbf{x}_3$ are the coordinates of the intersection between the wires and the image plane, in the calibration phantom coordinate system. ${}^{C}\mathbf{a}$ and ${}^{C}\mathbf{d}$ are coordinates of the intersection points of the middle wire (between **a** and **d** points) with the parallel side wires, in the calibration phantom coordinate system. **c** Intersection of the N-wires and the US image plane are automatically segmented. ${}^{U}\mathbf{x}_1, {}^{U}\mathbf{x}_2$, and ${}^{U}\mathbf{x}_3$ are the coordinates of the intersection between the top N-wire and the US image. Ratio of the $\mathbf{x}_3 - \mathbf{x}_1$ distance and the $\mathbf{x}_3 - \mathbf{x}_2$ distance is the same in the calibration phantom coordinate system as in the US image coordinate system; therefore, from the ${}^{U}\mathbf{x}_1, {}^{U}\mathbf{x}_2$ and ${}^{U}\mathbf{x}_3$ coordinates, the position of $\mathbf{x}_2$ point along the ${}^{C}\mathbf{a} - {}^{C}\mathbf{d}$ line can be determined, i.e., ${}^{C}\mathbf{x}_2$ coordinates can be computed

2. Scan conversion operation applied in curvilinear transducers provides equal horizontal and vertical US image pixel spacing, but using the method described in [3], it is not possible to constrain the calibration matrix to have equal pixel spacing.
3. In the method described in [3], the fiducial localization error is assumed to be isotropic, but this assumption is not valid, and therefore, the resulting calibration matrix is not optimal.

In this paper, we introduce an optimization method that does not assume isotropic fiducial localization error and the resulting calibration matrix can be constrained to be orthogonal and to have isotropic spacing. Notice that looking for an optimum in the desired space of parameters is better that obtaining an optimum in a more general space and then projecting to the desired space of parameters.

We evaluate the precision and accuracy of the N-wire-based methods described above so that they can be compared with other commonly used calibration methods.

Methods

According to [3], the probe calibration problem using an N-wire phantom can be formulated as:

$$ {}^{P}_{U}\mathbf{T}\,{}^{U}\mathbf{X} = {}^{P}\mathbf{X} \tag{2} $$

where the columns of the matrix ${}^{U}\mathbf{X}$ are the homogeneous coordinates of all the segmented middle wires in the *US* image coordinate system (z coordinate is considered as zero in the image plane) and the columns of ${}^{P}\mathbf{X}$ are the coordinates of the corresponding middle wires in the *Probe* coordinate system. This problem can be solved using least mean squares method.

Although the resulting calibration matrix is not optimal, we use it as an initial value for further optimization. The optimization step minimizes a cost function while ensuring orthogonality of ${}^{P}_{U}\mathbf{T}$.

We consider two different cost functions for the minimization:

- OPE (out-of-plane error):

$$ OPE = \sum_{i=1}^{N_i} \sum_{j=1}^{N_w} \left\| {}^{C}\mathbf{x}_{ij2} - {}^{C}\mathbf{x}^{p}_{ij2} \right\|^2 \tag{3} $$

where ${}^{C}\mathbf{x}_{ij2}$ refers to the intersection between the middle wire of the *j*-th N-wire of the phantom with the *i*-th image, expressed in the *Calibration Phantom* coordinate system

(computation is shown in Eq. 1). ${}^{C}\mathbf{x}^{P}_{ij2}$ is the projection of the segmentation of the same middle wire to the *Calibration Phantom* coordinate system using the ${}^{P}_{U}\mathbf{T}$ for that optimization step and the matrices ${}^{C}_{T}\mathbf{T}$ and ${}^{T}_{P}\mathbf{T}$ are provided by the Tracking System.

$$ {}^{C}\mathbf{x}^{P}_{ij2} = {}^{C}_{T}\mathbf{T}\,{}^{T}_{P}\mathbf{T}\,{}^{P}_{U}\mathbf{T}\,{}^{U}\mathbf{x}_{ij2} \tag{4} $$

N_i and N_w are the number of images taken and the number of N-wires in the phantom, respectively. Notice that this cost function is the same that is minimized in [3] by least mean squares method. The difference with the previous method is that in the additional optimization step, the structure of the image to probe matrix is constrained to have seven (isotropic scaling) or eight (anisotropic scaling) grades of freedom. The name was chosen by opposition to the following cost function.

- IPE (in-plane error):

$$ IPE = \sum_{i=1}^{N_i} \sum_{j=1}^{Nw} \sum_{k=1}^{3} \left\| {}^{U}\mathbf{x}_{ijk} - {}^{U}\mathbf{w}_{ijk} \right\|^2 \tag{5} $$

where:

- ${}^{U}\mathbf{x}_{ijk}$ is the intersection between the k-th wire of the j-th N-wire with the i-th US image, as appears on the ultrasound image.
- ${}^{U}\mathbf{w}_{ijk}$ is the expected intersection position of the k-th wire of the j-th N-wire with the computed image plane. To compute ${}^{U}\mathbf{w}_{ijk}$, we proceed as follows:
  1. Define ${}^{C}\mathbf{w}_{ijk}{}^{F}$ and ${}^{C}\mathbf{w}_{ijk}{}^{B}$ as the intersection of the k-th wire of the j-th N-wire with the front and back wall of the calibration phantom, respectively. Notice that all the intersections of the wires with the walls of the calibration phantom in the *Calibration Phantom* coordinate system are known because the calibration phantom is precisely manufactured.
  2. Express ${}^{C}\mathbf{w}_{ijk}{}^{F}$ and ${}^{C}\mathbf{w}_{ijk}{}^{B}$ in the US image coordinate system using the inverse of the ${}^{P}_{U}\mathbf{T}$ for that optimization step and the inverses of the matrices ${}^{C}_{T}\mathbf{T}$ and ${}^{T}_{P}\mathbf{T}$ provided by the Tracking System.
  3. Compute ${}^{U}\mathbf{w}_{ijk}$ as the intersection of the segment ${}^{U}\mathbf{w}_{ijk}{}^{F}$ ${}^{U}\mathbf{w}_{ijk}{}^{B}$ with the US image plane.

Terms involved in the computation are illustrated in Fig. 3.

In the IPE method, two changes are introduced with respect to the original method: a new cost function and also an optimization step. We introduced the OPE method to fairly compare the influence of the cost function. If we do not introduce the OPE method, we cannot determine if the improvement is due to the optimization step or due to the change in the cost function.

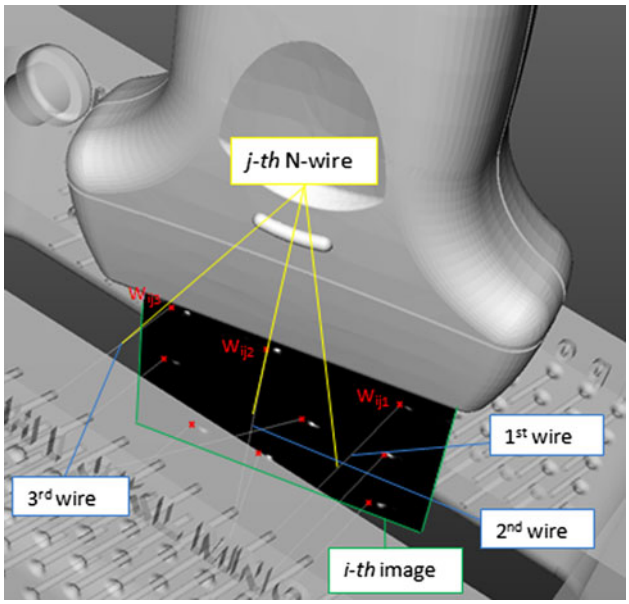

Fig. 3 Distance between the intersection of the wires with the computed image plane (*red points*) and their respective segmented points in the image (*white points*) is minimized

Main differences between the IPE and OPE metrics:

- In the OPE method, the ${}^{C}\mathbf{x}_{ij2}$ spatial positions of the middle wires are computed as a consequence of the similar triangles formed by the N-wires. In Eq. 1, it can be seen that the ratio used to make the computation is based on the intersections points visible in the US image and is expressed as

$$ \alpha_c = \frac{\left\| {}^{U}\mathbf{x_1} - {}^{U}\mathbf{x_2} \right\|}{\left\| {}^{U}\mathbf{x_1} - {}^{U}\mathbf{x_3} \right\|} \tag{6} $$

when in fact the proper ratio, based on the true intersection positions in the calibration phantom coordinate system, is

$$ \alpha = \frac{\left\| {}^{C}\mathbf{a} - {}^{C}\mathbf{x_2} \right\|}{\left\| {}^{C}\mathbf{a} - {}^{C}\mathbf{d} \right\|} = \frac{\left\| {}^{C}\mathbf{x_1} - {}^{C}\mathbf{x_2} \right\|}{\left\| {}^{C}\mathbf{x_1} - {}^{C}\mathbf{x_3} \right\|} \tag{7} $$

Due to the US image thickness, the bright spots of the fiducial wire intersection in the image are slightly blurred (particularly for the slanted middle wire), the ratio α_c may differ from α and therefore the ${}^{C}\mathbf{x}_{ij2}$ positions may be inaccurate. As we minimize the error in three dimensions, the inaccuracy along the axis parallel to the image normal may lead to inaccuracy in all directions.

- In the IPE method, the in-plane distance to all the wires is minimized. Some advantages of this approach are

- Positions of the wires with respect to the *Calibration Phantom* coordinate system are well known because the calibration phantom is precisely machined and the spatial positions used in the optimization do not depend on the slice thickness of the US image. The minimization does not rely on Eqs. 6 or 7, but each line intersection position is used individually and taken into account equally.
- Errors are only measured and minimized in-plane where the fiducial localization error is small. In contrast, with OPE method, the 3D position computed by Eqs. 6 and 7 may contain a large error component along the line of the middle wire.
- When using the IPE method, the error is estimated at all wire positions in the image, while with the OPE method the error is minimized only at the positions of the middle wire, near the center of the image. Therefore, the IPE method minimizes the error in a much larger image area, reducing tilting and rotation errors near the image boundaries of the field of view.

Calibration was evaluated using both cost functions. The cost function was minimized by using Levenberg Marquard iterative nonlinear optimization algorithm. The closed-form solution proposed in [3] was used as an initial value. Rotation was parameterized using quaternions.

Calibration transformation modeling

According to the model described in [6], the calibration transformation ${}^{\mathbf{P}}_{\mathbf{U}}\mathbf{T}$ that we are looking for is the composition of two transformations: a rigid transformation that place the scan plane with respect to the markers attached to the probe and a scaling transform that converts form pixels units to mm.

The calibration method could be extended to identify geometric distortions in the image (such as linear skew or nonlinear deformations), trying to recover errors in the scan conversion method of the scanner. However, adding more unknown variables to the optimization can lead to decreased accuracy and robustness if input images are imperfect.

We choose to identify image pixel size by the calibration method, as it is not always possible to retrieve these values from the US scanner and the values may be also changed during capturing of the displayed image from the scanner.

To consider the possibility of isotropic and anisotropic scaling (same or different horizontal and vertical scale in the image plane), both methods were evaluated using 7 and 8 parameters (3 rotation + 3 translation + 1 or 2 scale).

In all the experiments described in "Results and discussion" probe calibration was performed by the following methods:

- NOPT (no optimization): closed-form calibration solution proposed by [3].
- OPEI (out-of-plane error, isotropic image scaling): 7 parameters (3 rotation, 3 translation and 1 scale) were optimized using the OPE cost function.
- OPEA (out-of-plane error, anisotropic image scaling): 8 parameters (3 rotation, 3 translation and 2 scale) were optimized using the OPE cost function.
- IPEI (in-plane error and isotropic image scaling): 7 parameters were optimized using the IPE cost function.
- IPEA (in-plane error and anisotropic image scaling): 8 parameters were optimized using the IPE cost function.

From the limited description that is provided in [2], it may be possible that the authors used the OPEI and OPEA methods. To the best of our knowledge, this is the first time that IPEI and IPEA methods are proposed to solve the ultrasound calibration problem using an N-wire phantom.

Calibration quality assessment

Following the recommendations in [6], the calibration results (ultrasound image to probe transformations) were assessed in terms of precision and accuracy using the procedures described below.

Precision test procedure

To compute the precision of a calibration method, N independent calibrations are performed with that method. The result is a set of N transformations ${}^{\mathbf{P}}_{\mathbf{U}}\mathbf{T_i}$ with $i = 1 \ldots N$.

Five specific points of the image (center and the four corners) are mapped to the *Probe* coordinate system through these N transformations (see Fig. 4). If the method is precise, the point positions mapped into the *Probe* coordinate system are almost identical in all the trials.

The metric used to quantify the precision of a method is the **calibration reproducibility (CR).** If we call ${}^{\mathbf{U}}\mathbf{x}$ the point in the image mapped to space using the *i*-th *US Image* to *Probe* transformation, then the CR is defined [6] as:

$$CR = \frac{1}{N}\sum_{i=1}^{N}\left\| {}^{\mathbf{P}}\bar{\mathbf{x}} - {}^{\mathbf{P}}_{\mathbf{U}}\mathbf{T_i}\,{}^{\mathbf{U}}\mathbf{x}\right\| \tag{8}$$

where ${}^{\mathbf{P}}\bar{\mathbf{x}}$ is the centroid

$${}^{\mathbf{P}}\bar{\mathbf{x}} = \frac{1}{N}\sum_{i=1}^{N}{}^{\mathbf{P}}_{\mathbf{U}}\mathbf{T_i}\,{}^{\mathbf{U}}\mathbf{x} \tag{9}$$

This is a measure solely based on calibration (does not incorporate the errors from the position sensor, the segmentation in the image, etc.). This method is becoming the standard way of assessing precision of a calibration procedure [6].

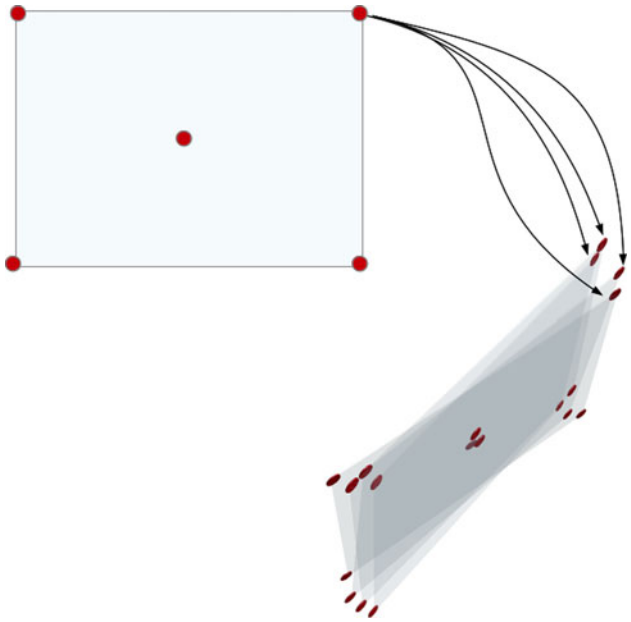

Fig. 4 Precision test. The selected points (*center* and *corners*) are mapped through multiple ${}^{\mathbf{P}}_{\mathbf{U}}\mathbf{T_i}$ transformations computed from repeated calibrations with the same method. If the method is precise, the mapped positions of the selected image points should be near across all the trials

Accuracy test procedure

To compute the accuracy of a calibration method, N independent calibrations are performed with the same method. The result is a set of N transformations.

Then, a point target in a *Reference* coordinate system is scanned with ultrasound. This point is determined by the intersection of two straight wires (cross-wire) as illustrated in Fig. 5a. The coordinates of the point that appears in the *US image* are then transformed to the *Reference* coordinate system using the N different calibration matrices.

The result of each repeated calibration is slightly different; therefore, the transformed point is mapped to slightly different positions in the *Reference* coordinate system, as shown in Fig. 5b.

The only condition for the *Reference* coordinate system is that it must remain fixed with respect to the cross-wire during all the experiment. However, the calibration phantom should not be reused as a *Reference* coordinate system to test the accuracy, because it may introduce a bias. In our experiment, the *Reference* coordinate system is linked to an optical marker that is rigidly attached to the box that contains the cross-wire.

The metric used to compute the accuracy of each of the N transformations is the **point reconstruction accuracy (PRA)**. PRA is defined [10] as

$$PRA = \left\| {}^{\mathbf{R}}\mathbf{x} - {}^{\mathbf{R}}_{\mathbf{T}}\mathbf{T}^{\mathbf{T}}_{\mathbf{P}}\mathbf{T}^{\mathbf{P}}_{\mathbf{U}}\mathbf{T}\,{}^{\mathbf{U}}\mathbf{x} \right\| \tag{10}$$

where ${}^{R}\mathbf{x}$ is the position of a point with respect to the *Reference* coordinate system (usually measured by using a stylus), ${}^{\mathbf{U}}\mathbf{x}$ is the position of the same point in the *US image*, ${}^{\mathbf{P}}_{\mathbf{U}}\mathbf{T}$ is the *US image* to *Probe* transformation obtained during calibration and ${}^{\mathbf{T}}_{\mathbf{P}}\mathbf{T}$, ${}^{\mathbf{R}}_{\mathbf{T}}\mathbf{T}$ are, respectively, the *Probe* to *Tracker* transformation and *Tracker* to *Reference* transformation provided by the tracking system.

To evaluate the accuracy of the system with the shallow probe, a cross-wire was scanned in different regions of the image (center and 4 corners). The segmentation of the cross-wire was done manually. Since determining the position of the wire intersection on a single frame is difficult due to the slice thickness, a video sequence was acquired while continuously traversing back and forth over the wire crossing (see Fig. 6). In order to achieve as accurate out-of-plane localization as possible, the frame that is centered on the intersection point was determined by inspecting the 3D volumetric

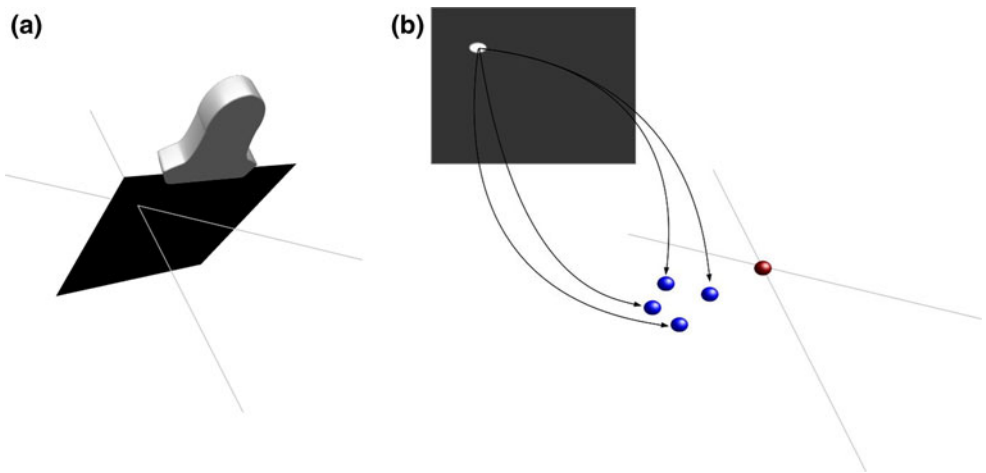

Fig. 5 **a** Scanning of a cross-wire. **b** The point in the image is mapped to the space using different transformations computed with the same method. *Blue*: transformed points, *Red*: ground-truth point

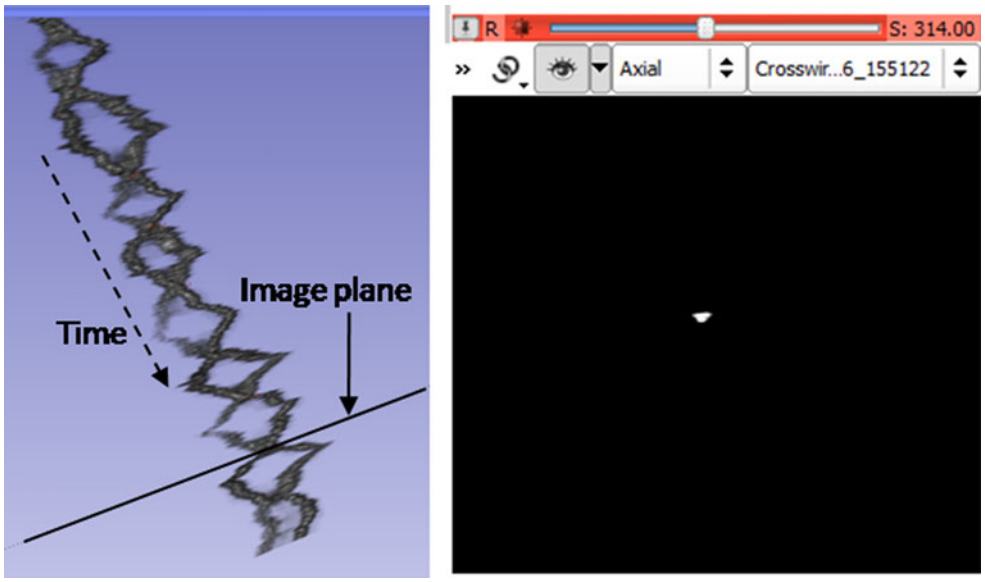

Fig. 6 A volumetric image was generated from the sequence of US frames by stacking the frames with 1 mm spacing. Then the volume was rendered in three dimensions using 3D Slicer [14]. The three-dimensional visualization helped to identify the image plane of the wire intersection. The intersection point was marked in the two-dimensional view of the selected image plane. In this video, the image plane intersected the cross-wire 9 times. Each intersection is observed as a white spot in the axial view of 3D Slicer

reconstruction of the sequence. In the 3D reconstruction, two dimensions are the two spatial dimensions of the image and the third dimension is the time, therefore, the back and forth motion creates a sinusoid pattern. The wire intersection position was then manually marked on the selected frame.

The ground-truth position of the wire intersection point in the *Reference* coordinate system was obtained by using the calibrated stylus that is part of the Polaris Spectra kit. The tip position of the stylus was acquired ten times, while touching the cross-wire and then those positions were averaged.

Notice that PRA provides an estimation of the whole system error. It includes not only the calibration error but also other errors that are not negligible, especially misalignment of the scan plane with the point phantom, tracker error, image segmentation and stylus calibration. This implies that an objective comparison of calibration accuracy between different methods requires the usage of exactly the same hardware devices, experimental setup and settings.

Data collection

Experiments were performed with the Polaris Spectra optical tracker (Northern Digital Inc, Waterloo, Ontario, Canada) and passive markers. A SonixTOUCH machine (Ultrasonix Medical Corporation, Richmond, BC, Canada) machine with an image resolution of 820 × 616 pixels was used for the acquisition of B-mode US images. The probes used were a L14-5/38 Ultrasonix linear transducer with a 3 cm depth at 10 MHz (*shallow probe*) and a C5-2/60 Ultrasonix convex transducer with a 15 cm depth at 5 MHz (deep probe).

For each of the probes, 10 independent video sequences of typical calibration procedures were acquired. Each video sequence contains over 400 hundred image frames in which the wires of the calibration phantom were automatically segmented using [7]. From each video sequence, 5 sets of 80 frames were randomly drawn. Thus, for each probe, there are 50 sets of 80 images. Those sets were used to compute the calibration transformations with the different methods described above.

Data was collected using the PLUS (Public software Library for UltraSound imaging research) toolkit [7].

Results and discussion

Precision

Precision was evaluated for 5 different calibration methods, using both the shallow and the deep probe. Calibration reproducibility was estimated for the center of the image and also for the corners using ten different sequences. The results are summarized in Tables 1 and 2 for the shallow and deep probes, respectively.

In-plane minimization yielded better precision results using both probes, but the difference with the closed-form solution and the out-of-plane methods is more significant when using the deep probe. This may be explained because

Table 1 Precision analysis (CR) in the center and average (center + 4 corners) of the image for the *shallow probe*

	Center		Average	
	Mean (mm)	SD (mm)	Mean (mm)	SD (mm)
NOPT	0.52	0.12	0.83	0.35
OPEI	0.53	0.12	0.83	0.34
OPEA	0.53	0.11	0.83	0.34
IPEI	0.51	0.12	0.77	0.34
IPEA	0.50	0.12	0.69	0.31

Table 2 Precision analysis in the center and average (center + 4 corners) of the image for the *deep probe*

	Center		Average	
	Mean (mm)	SD (mm)	Mean (mm)	SD (mm)
NOPT	0.72	0.22	2.96	2.47
OPEI	0.70	0.17	2.60	2.16
OPEA	0.72	0.20	2.85	2.20
IPEI	0.56	0.18	2.05	1.70
IPEA	0.56	0.16	1.99	1.61

with the shallow probe the thickness of the US beam is shorter than with the deep probe, and therefore, the middle wire intersection with the US image (${}^{C}\mathbf{x}_2$) can be computed more reliably. The advantage of using all the wires can be observed in the better precision in the corners of the image.

Although precision with the deep probe was considerably improved with the in-plane minimization, we think that it may be further improved in the future. Calibration phantom used has only three N-wires and the maximum distance between wires is 2 cm. Therefore, the region of the image covered by the phantom when using a deep probe is quite small and results may be dependent on the movement of the phantom with respect to the probe during calibration. This is reflected in the high standard deviation of the CR for the deep probe. Nonetheless, improvement in CR with the proposed optimization method in this difficult scenario was about 20 % in mean and also in standard deviation.

Accuracy

The PRA using the shallow probe for images captured near the center of the B-scan as well as the mean of every point captured is given in Table 3. The PRA distribution for the in-plane methods and the NOPT method is shown in Fig. 7.

Notice that the same cross-wire segmentation is used for all the methods so the error is not expected to bias the results. With the shallow probe the cross-wire segmentation error can be roughly estimated to 5 pixels. The typical scale is 0.05 mm/pixel. Therefore, the in-plane error in the segmen-

Table 3 Accuracy (PRA) of the whole system was analyzed for the center of the image and also for the corners using a cross-wire phantom and the shallow probe

	Center		Average	
	Mean (mm)	SD (mm)	Mean (mm)	SD (mm)
NOPT	1.11	0.13	1.36	0.59
OPEI	1.11	0.13	1.36	0.59
OPEA	1.12	0.13	1.36	0.61
IPEI	1.02	0.12	1.20	0.36
IPEA	1.03	0.12	1.18	0.38

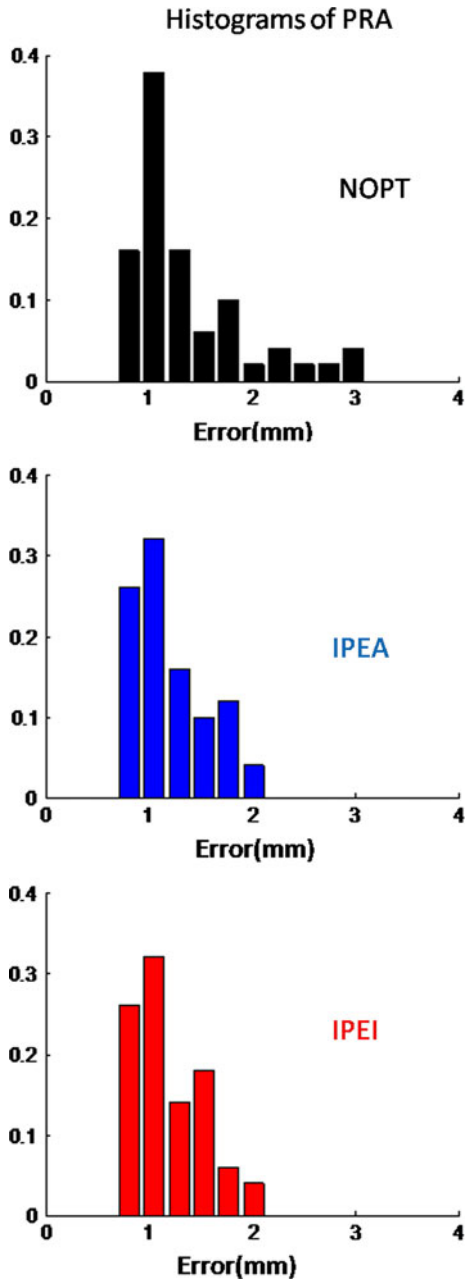

Fig. 7 PRA histogram for the different methods using the shallow probe

Table 4 p value of the Wilcoxon signed-rank test for paired samples that compare the PRA results (average of center and corners) using the NOPT method with the PRA results obtained with the in-plane methods

	NOPT versus IPEI	NOPT versus IPEA
p value	0.023	0.003

tation of the cross-wire is estimated around 0.25 mm with the shallow probe.

Among the implemented methods, the best results were obtained with the in-plane methods. In order to know if the improvement of the proposed in-plane methods (IPEI and IPEA) is significant, a statistical analysis was performed. The Wilcoxon signed-rank test for paired samples was performed to compare the PRA results using the NOPT method with the PRA results obtained with the in-plane methods. As the PRA values are paired, it is possible to compute the difference between the PRA values obtained using the NOPT method and the corresponding values using IPEI or IPEA. The null hypothesis of the test is that the median of the computed differences is zero. Results are shown in Table 4.

The p values are well below the commonly used 0.05 value; therefore, the improvement in accuracy of the proposed optimization method can be considered significant.

Regarding the comparison with other methods reported in literature [6], the numerical values that we get are slightly better but we cannot tell that the scenario in which experiments were performed is exactly the same. Therefore, the comparison with other reported methods is not straightforward. Despite we used the same type of probe and the same depth to make the results comparable, we do not have other important information such as the frequency of the probes or details of the procedure they used (e.g., segmentation strategy).

In addition to the good results, the N-wire-based method has several advantages over the alternative methods. N-wire-based method requires just a short continuous US image acquisition while translating the probe back and forth over the phantom a couple of times, which even inexperienced operators can perform without any difficulty. No manual processing of the images is needed. The calibration phantom can be easily reproduced by using a 3D printer and threading nylon wire (such as fishing line) through the designated holes.

Implementation

The software that implements the above described calibration methods along with source code, documentation, tutorials, test data, automatic tests, description and CAD model of the calibration phantom are all available as part of the PLUS (Public software Library for UltraSound imaging research) toolkit [7]. This toolkit is developed by the Laboratory for Percutaneous Surgery (PerkLab) at Queens University (Ontario, Canada) and is available freely, without any restrictions at [5].

Conclusions

The proposed optimization in the computational methodology of N-wire-based US calibration improved mean accuracy by 10 % and precision by 8 %. It was also shown that the improvement in accuracy is statistically significant.

Based on our experiments, the performance of N-wire-based method with the proposed computational enhancement is better or at least comparable to previously reported alternative calibration methods. However, the simplicity of fabricating the calibration phantom, of acquiring the images and the fully automatic processing may make the N-wire-based method a more favorable calibration option compared to the others.

The implementation of the proposed computational method has been made freely available as part of the PLUS toolkit [7].

Acknowledgments This work was supported in part by Agencia Nacional de Investigacion e Innovacion (ANII, Uruguay) under grant (BE POS 2010 2236). Comision Sectorial de Investigacion Cientıfica (CSIC, Universidad de la Republica, Uruguay) supported the internship of G. Carbajal at Perklab. This work was co-funded as an Applied Cancer Research Unit of Cancer Care Ontario with funds provided by the Ontario Ministry of Health and Long-Term Care. G. Fichtinger is supported as a Cancer Care Ontario Research Chair.

Conflict of interest None.

References

1. Brown RA et al (1979) A stereotactic head frame for use with CT body scanners. Inves Radiol 14(4):300
2. Chatrasingh M, Suthakorn J, Ongwattanakul S, Wiratkapun C, Shuijantuq S Ultrasound calibration toolkit with a high-adjustability feature based on user requirements
3. Chen TK, Thurston AD, Ellis RE, Abolmaesumi P (2009) A real-time freehand ultrasound calibration system with automatic accuracy feedback and control. Ultrasound Med biol 35(1):79–93
4. Comeau RM, Fenster A, Peters TM (1998) Integrated MR and ultrasound imaging for improved image guidance in neurosurgery. In: Medical Imaging'98, pp 747–754. International Society for Optics and Photonics, San Francico
5. Laboratory for Percutaneous Surgery (PerkLab) at Queen's University. Plus (public software library for ultrasound imaging research). Internet development repository, http://plustoolkit.org. Accessed January (2013)
6. Hsu P-W, Prager RW, Gee AH, Treece GM (2007) Freehand 3d ultrasound calibration: A review. Technical report. University of Cambridge, Cambridge
7. Lasso A, Heffter T, Pinter CS, Ungi T, Fichtinger G (2012) Implementation of the PLUS open-source toolkit for translational research of ultrasound-guided intervention systems. The MIDAS Journal—Systems and Architectures for Computer Assisted Inter-

ventions 2012, Workshop at Medical Image Computing and Computer-Assisted Intervention (MICCAI 2012), pp 1–12, http://hdl.handle.net/10380/3367
8. Lee S, Fichtinger G, Chirikjian GS (2002) Numerical algorithms for spatial registration of line fiducials from cross-sectional images. Med Phys 29:1881
9. Lindseth F, Tangen GA, Lango T, Bang J et al (2003) Probe calibration for freehand 3D ultrasound. Ultrasound Med Biol 29(11):1607
10. Mercier L, Lang T, Lindseth F, Collins LD (2005) A review of calibration techniques for freehand 3D ultrasound systems. Ultrasound Med Biol 31(2):143–165
11. Muratore DM, Galloway RL (2001) Beam calibration without a phantom for creating a 3D freehand ultrasound system. Ultrasound Med Biol 27(11):1557–1566
12. Pagoulatos N, Haynor DR, Kim Y (1999) Fast calibration for 3D ultrasound imaging and multimodality image registration. In: Engineering in Medicine and Biology, 1999. 21st Annual Conf. and the 1999 Annual Fall Meeting of the Biomedical Engineering Soc., BMES/EMBS Conference, 1999. Proceedings of the First Joint, vol 2, p 1065
13. Prager RW, Rohling RN, Gee AH, Berman L et al (1998) Rapid calibration for 3D freehand ultrasound. Ultrasound Med Biol 24(6):855
14. Pieper S, Halle M, Kikinis R (2004) 3D SLICER. In: Proceedings of the 1st IEEE International Symposium on Biomedical Imaging: From Nano to Macro, pp 632–635